Thin Solid Films 770 (2023) 139763

Contents lists available at ScienceDirect

Thin Solid Films

journal homepage: www.elsevier.com/locate/tsf

Structure, magnetic morphology and magnetization correlations in pulsed laser deposited $CoFe_2O_4$(111) thin films

Avisek Das [a,1], Annarose J Palliyan [a,1], Ajit Kumar Sahoo [b], Jyoti Ranjan Mohanty [b], Venkataiah Gorige [a,*]

[a] School of Physics, University of Hyderabad, Gachibowli, Hyderabad, 500046, Telangana, India
[b] Department of Physics, Indian Institute of Technology Hyderabad, Kandi, Sangareddy, 502285, Telangana, India

ARTICLE INFO

Keywords:
Cobalt ferrite
Thin films
Raman spectroscopy
Cation distribution
Coercivity
Magnetic anisotropy

ABSTRACT

The present paper reports a complete study on the correlation between structure, morphology, and magnetic properties of (111)-oriented cobalt ferrite ($CoFe_2O_4$) thin films with varying film thickness. The $CoFe_2O_4$ (CFO) thin films were deposited on Pt-coated Si substrate by pulsed laser deposition (PLD) at 550 °C. The x-ray diffraction (XRD) data confirms the (111)-oriented growth of the cobalt ferrite films. The in-plane morphology of the films in the field emission scanning electron micrographs ensure the Stranski–Krastanov growth mechanism, and the atomic force micrographs confirms the effect of lattice relaxation on the morphology of the films with varying thickness. The possible cation distributions for the samples were determined from the Raman spectroscopy, which revealed the crystal structure-magnetic property correlations in cobalt ferrite films. The magnetic hysteresis ($M-H$) loops show a significant spin reorientation by showing the variation between the in-plane (IP) and out-of-plane (OP) magnetization. The presence of a kink on the OP $M-H$ loops and its variation with film thickness clearly establishes the existence of competing magnetic anisotropies in the films. The high coercivity (H_C) values observed for OP magnetization of cobalt ferrite films with thicknesses 115 nm and 125 nm may be explored for possible room-temperature (RT) device applications.

1. Introduction

Magnetic oxide materials have gained significant attention in recent past on account of their intriguing physical properties and potential device applications [1]. The room-temperature ferrimagnetic oxide thin films, having distinct magnetic responses, are of immense concern owing to the tunability of their properties suitable for device applications [2]. Cobalt ferrite, $CoFe_2O_4$, having an inverse spinel structure, belonging to the magnetic ferrite family, is one among such oxide thin films with high coercivity and considerable magnetization [3]. Owing to their high magnetic coercivity, magnetic anisotropy, high Curie temperature (T_C) and chemical stability, ferrites are promising systems for high density magnetic storage and recording [4–7]. The cobalt ferrite thin films are also widely used as spin filters and pinning layers in magnetic tunnel junctions and spin valve structures [8]. Interestingly, cobalt ferrite with space group $Fd\bar{3}m$, have Co^{2+} and Fe^{3+} ions of which 50% of the Fe^{3+} ions along with Co^{2+} ions fill the octahedral (O_h) sites whereas the other 50% of Fe^{3+} ions fill the tetrahedral (T_h) sites, giving rise to the net magnetization in cobalt ferrite [9].

The magnetization of cobalt ferrite thin films rely not only on the cation distribution but also on the substrate, film thickness, interfacial strain, lattice mismatch effect at the substrate–film interface, etc. In view of these complexities, several studies have been carried out involving thin films of cobalt ferrite. Studies related to the growth of cobalt ferrite films on different substrates like Au, Ru, W, etc. were carried out by various research groups [10,11]. Later it was reported that the deposition of the cobalt ferrite films on a hexagonal single crystal substrate, Ru(0001), using molecular beam epitaxy led to the growth of oriented crystallites [12]. The cobalt ferrite films deposited on a silicon wafer were reported to have a larger coercivity of 0.7 T, enhancing the magnetization of the samples [13]. Investigations on the thickness dependence of magnetic properties were carried out by depositing cobalt ferrite films on a quartz substrate where the magnetization reduced considerably with film thickness [14]. The cobalt ferrite(111) films of thickness 200 nm deposited on α-Al_2O_3(0001) substrate and on Pt(111) were reported to show strong IP anisotropy [15]. Also, films with lesser thickness were found to form smaller particles which directly influence various properties of the materials [16]. The magnetization

* Corresponding author.
E-mail address: vgsp@uohyd.ac.in (V. Gorige).
[1] Contributed equally to this work.

https://doi.org/10.1016/j.tsf.2023.139763
Received 10 November 2022; Received in revised form 23 February 2023; Accepted 24 February 2023
Available online 1 March 2023

studies of the cobalt ferrite films on $SrTiO_3$(001) are reported to show significantly high magnetization and coercivity values, attributed to the compressive strain. In contrast, films on MgO(001) shows weak magnetic behavior due to the tensile strain at the film–substrate interface [17]. Although many reports are seen in the literature, an extensive investigation on the effect of interfacial strain on the physical properties, particularly on magnetization, has not been explored yet.

In this regard, a study on the growth of cobalt ferrite films with varying thickness was carried out by depositing thin films on a Pt-coated Si substrate by using PLD technique. The structural and morphological studies were performed by XRD, field emission scanning electron microscopy (FESEM), magnetic force microscopy (MFM), and atomic force microscopy (AFM). A thorough structure-magnetic correlations were established by performing Raman spectroscopy. The magnetization was investigated to understand the competition between different magnetic anisotropies of the film and to verify their suitability for possible device applications at RT.

2. Experimental details

The cobalt ferrite thin films with compositional formula $CoFe_2O_4$ were deposited on platinum (Pt-) coated silicon substrate by PLD technique. The reason for choosing Pt-coated Si substrate in the present case is to promote the oriented growth of cobalt ferrite, as the lattice parameter of cobalt ferrite is nearly equal to twice the lattice parameter of Pt [18]. The cobalt ferrite films with varying thicknesses were deposited by using a KrF excimer laser with 248 nm wavelength, 1.15 J/cm^2 fluence, and 5 Hz repetition rate by maintaining the substrate 4 cm away from the target. The films were deposited at the rate of 1.1 Å/s. Prior to the film growth, the base pressure of the deposition chamber was maintained at 0.3 mPa. The substrate temperature and oxygen (O_2) partial pressure were maintained at 550 °C and 0.173 mPa, respectively. The samples were in situ annealed at 650 °C in an O_2 partial pressure of 0.3×10^{-5} Pa for 2 h. The samples with thicknesses 115 nm, 125 nm, 160 nm, 175 nm, 250 nm, and 300 nm are designated hereafter as CFO-115, CFO-125, CFO-160, CFO-175, CFO-250, and CFO-300, respectively. The structural characterization of all samples was performed by using the x-ray diffractometer (PANalytical X'Pert3) with Cu-Kα radiation source in out-of-plane ($\theta-2\theta$) configuration. The morphological and compositional studies were performed by using the FESEM (CARL-ZEISS ULTRATM-55) at an operating voltage of 5 kV. The FESEM was equipped with an energy dispersive x-ray (EDS) spectrometer. During the EDS measurements, the electrons were accelerated at 5 kV with a beam current of 2.27 A for an aperture size of 120 μm and the probe current was found to be 9.3 nA. The Raman measurements were carried out using the scanning near-field optical microscope coupled with the micro-Raman instrument (WITech, Alpha 300) equipped with Nd:YAG laser with wavelength 532 nm. The magnetic and surface topography of the deposited films were studied by analyzing MFM and AFM images recorded using (Bruker's MESP-V2) microscope. The IP and OP magnetic hysteresis ($M-H$) loops were carried out by vibrating sample magnetometer (LakeShore' 7410, USA) in an applied field range, $0-\pm1.5$ T.

3. Results and discussion

3.1. X-ray diffraction

XRD is regarded as one of the best suitable techniques for phase identification and structural characterization of materials. In the present investigation, the deposited cobalt ferrite films with different thickness were subjected to XRD measurements at RT and the corresponding XRD patterns are shown in Fig. 1. From the figure, it is noticed that there are two categories of peaks corresponding to the substrate and cobalt ferrite films, respectively. The peaks corresponding to the substrate are identified with the '*' mark, and the cobalt ferrite-related

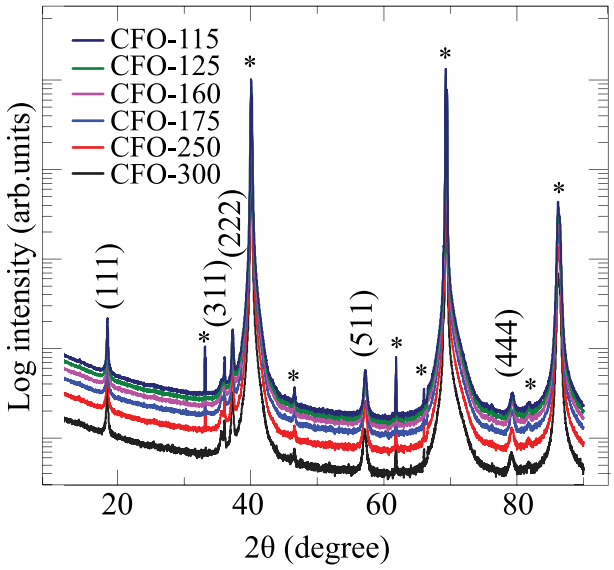

Fig. 1. The x-ray diffraction patterns of CFO thin film samples. The '*' mark in patterns represents the peaks corresponding to the Pt-coated Si substrate.

peaks are identified with their respective (hkl) planes. After a close observation, it is clear that the single-phase cobalt ferrite films oriented along [111] direction are formed with no detectable secondary phases. The preferred growth in this particular direction is due to the least surface energy of the (111) planes of spinel ferrites [19]. The intensity of the peaks representing the substrate is invariant, whereas the intensity of all the peaks corresponding to cobalt ferrite shows a linear increase with the film thickness. Although the thickness of the films was varied systematically, no noteworthy shift in the peak positions was observed, which plausibly hints at the presence of a non-uniform strain due to the interdependence of structural and magnetic interactions of the atoms present in these samples. The present observation is in agreement with the reported literature [20].

With a view to understanding the interfacial lattice strain in the deposited films, the percentage of lattice mismatch (δ) between the thin films and platinum-coated silicon substrate was estimated by the equation,

$$\delta = \frac{2a_{Pt} - a_{CFO}}{a_{CFO}} \times 100 \quad (1)$$

where a_{Pt} and a_{CFO} are the lattice parameters of platinum (a_{Pt} = 3.9201 Å) and cobalt ferrite bulk (a_{CFO} = 8.3869 Å) respectively [21]. The value of δ is found to be −6.5% indicating the existence of a compressive strain in the thin films. As the thermal expansion coefficients of Pt and cobalt ferrite are different at post annealing temperature (650 °C) and may generate the significant strain at the interface thereby resulting in impact on the morphology of films [18].

In order to know more about the dependence of lattice parameters on thickness and strain of the films, lattice parameters were calculated and tabulated in Table 1. It is noticed that there is an overall increase in the lattice parameter with the increase of film thickness. This behavior can be ascribed to the relaxation of strain with increase in film thickness. The estimated δ values are enlisted in Table 1. In general, due to the lattice mismatch, a huge lattice strain (ε) at the interface may be generated, and the strain experienced by the films was quantified using the formula,

$$\varepsilon = \frac{a_{film} - a_{bulk}}{a_{bulk}} \times 100 \quad (2)$$

here a_{film} and a_{bulk} are the lattice constants of cobalt ferrite film and bulk counterpart (a_{bulk} = 8.3869 Å), respectively [21]. With the

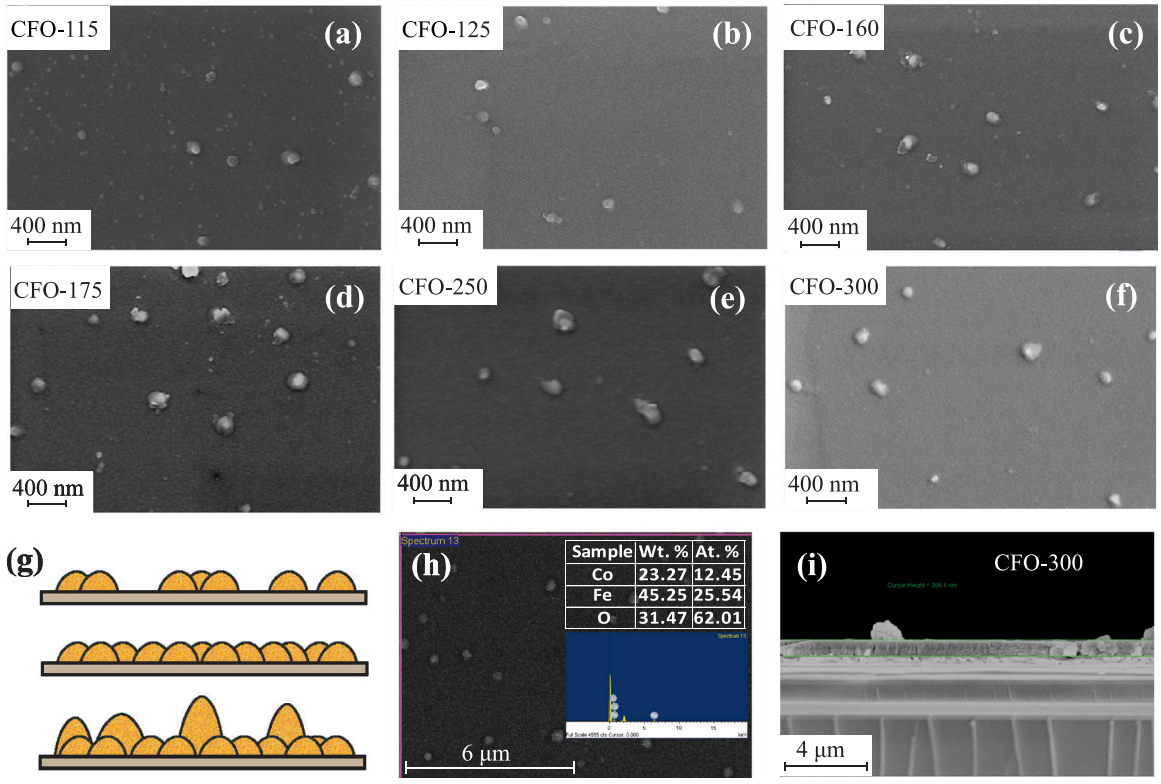

Fig. 2. (a–f) The FESEM micrographs of CFO thin film samples, (g) schematic representation of Stranski–Krastanov film growth, (h) elemental mapping for a typical CFO film, and (i) cross-sectional FESEM image of CFO-300 film.

Table 1
The values of lattice parameter (a_{film}), the percentage of lattice mismatch (δ), the percentage of lattice strain (ϵ), crystallite size (D) and strain due to crystallization (η) of the CFO thin film samples. The values mentioned in the parenthesis represent the estimated standard deviation of the corresponding parameter.

Sample code	a_{film}(Å)	δ	ϵ	D (nm)	η
CFO-115	8.311(9)	−5.677(4)	−0.681(1)	40(4)	0.008(9)
CFO-125	8.309(2)	−5.646(8)	−0.713(4)	80(0)	0.011(1)
CFO-160	8.314(7)	−5.709(2)	−0.647(6)	40(4)	0.007(2)
CFO-175	8.317(7)	−5.743(2)	−0.611(8)	180(4)	0.011(1)
CFO-250	8.317(2)	−5.737(5)	−0.617(8)	185(2)	0.011(1)
CFO-300	8.327(3)	−5.851(8)	−0.497(1)	100(2)	0.012(7)

enhancement of film thickness, it is observed that there is an increase in a_{film}, and the values tend to a_{bulk} value. The decrease in strain with increase in film thickness gives an impression that the thicker films are more lattice relaxed than thinner ones. It can also be concluded that the strain experienced by the film is compressive in nature. In addition, the lattice strain experienced by the film is also manipulated by the crystallization and orientation of the films. Therefore, the net strain due to crystallization and the crystallite size of the films were determined by employing the Williamson–Hall method given by the equation,

$$\beta cos\theta = \frac{\lambda}{D} + \eta sin\theta \tag{3}$$

and are listed in Table 1. Though there is an overall increase in the crystallite sizes, a minimal variation in the strain is only observed for higher film thicknesses. This might be due to the different crystallization growths happening in different directions and the competition between the strain caused due to crystallization and interface lattice mismatch.

3.2. Surface morphology

3.2.1. FESEM

With a view to understanding the nature of surface of films, FESEM was carried out for all the samples, and the corresponding micrographs are shown in Fig. 2(a–f). A 3-dimensional cluster kind of growth, referred as Stranski–Krastanov growth (schematically represented in Fig. 2(g)), is anticipated in all the FESEM images. The film growth pace is determined by the deposition of constituent atoms of the film over the substrate or pre-existing clusters [22]. The size of the clusters seem to be increasing with an increase in film thickness. The balance between the growth and disintegration of the cluster is determined by the overall behavior of its free energy. For a particular cluster size, a positive derivative of free energy with respect to constituent atoms of the cluster confirms the instability of the cluster, and its dissolution takes place thereafter. However, in the present case, as the cluster size increases, the derivative is negative, the cluster is found to be stable, and the growth of the cluster is dominating over dissolution [23].

The compositional quality of the deposited films was confirmed by performing the EDS measurements for all the films, and a typical EDS spectrum is presented in Fig. 2(h). The composition of the constituent elements estimated from the EDS data is in good concurrence with the nominal composition of the cobalt ferrite, which confirms the compositional quality of the prepared thin films. To know the multidimensional aspects of the film and the clusters, a cross-sectional FESEM was performed on the films, and a typical FESEM image is depicted in Fig. 2(i). The figure, infers that the thickness of the film is determined to be 300 nm and it is consonant with the thickness measured from surface profilometer. The clusters seen in the cross-sectional FESEM confirm the 3-dimensional nature of the clusters.

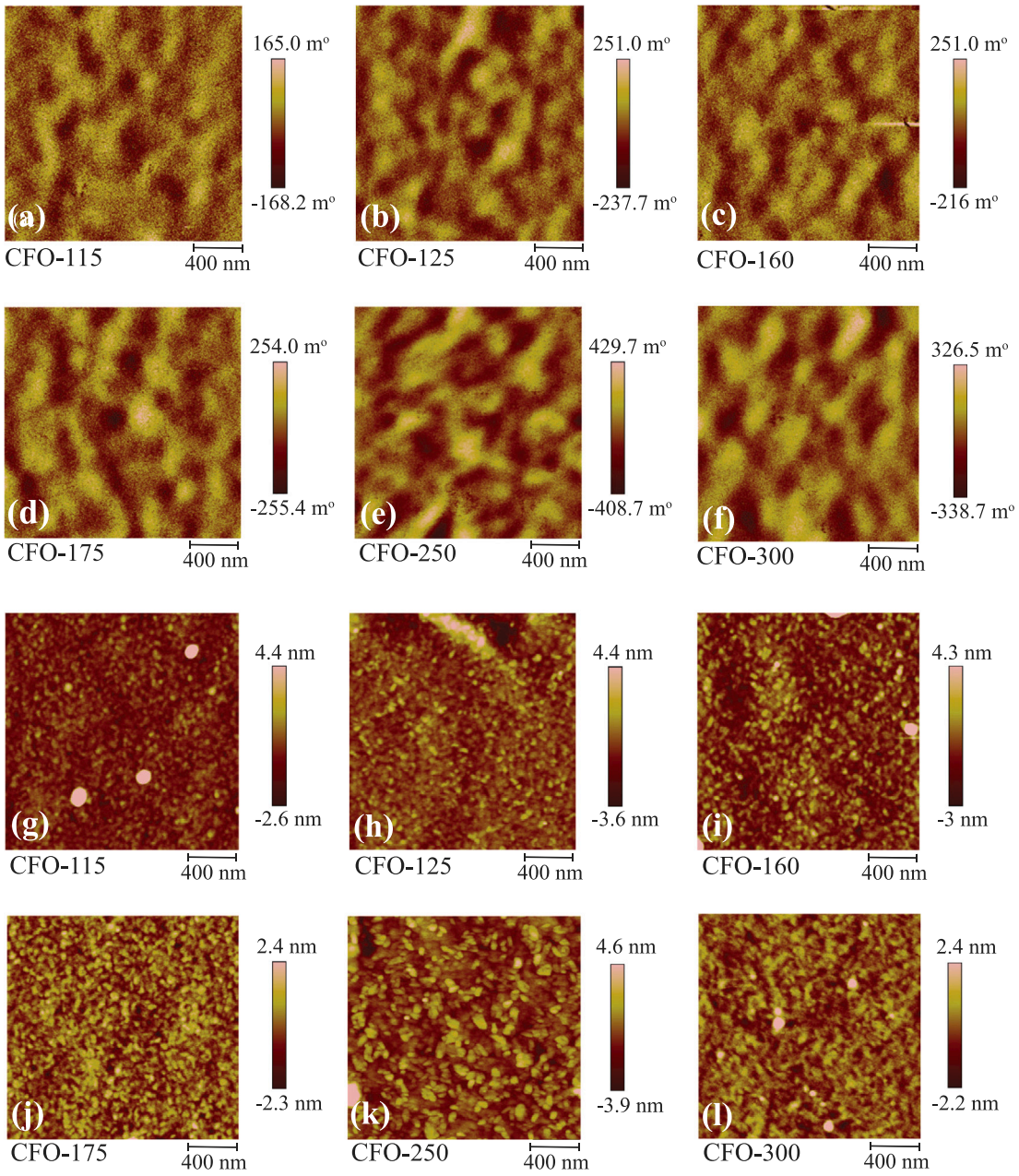

Fig. 3. (a–f) The MFM and (g–l) AFM images of CFO thin film samples.

3.2.2. MFM and AFM

As the surface morphology was analyzed, it is important to look into the magnetic morphology of the samples to understand the nature of the domains in them. Therefore MFM images were recorded and are presented in Fig. 3(a–f). The micrographs show that the bright and dark spots refer to the repulsive and attractive magnetic force gradient, respectively. The magnetic domains were found to exhibit two different contrasts in the images. The size of domains was assessed quantitatively by the line scan at various points, and the corresponding parameters are given in Table 2. It has been observed that the magnetic domains are of an irregular band-like nature. As the thickness of the film increases, the magnetic phase difference (MPD) is found to increase substantially, and for the CFO-300 film, the MPD value is two times that of the CFO-115 film. As the MFM probes the OP signal, the OP contrast could be correlated to the MPD in the MFM images of the films. For an increasing film thickness, the OP magnetic contrast is also found to increase by enhancing the magnetization of the films. The domain size growth observed for the films may be attributed to the increased thickness due to fast deposition at higher temperatures [22].

Table 2
The values of magnetic phase difference (MPD), magnetic domain width (W_D) and surface roughness (R_q) of the CFO thin film samples.

Sample code	MPD (±2 m°)	W_D (±5 nm)	R_q (±0.5 nm)
CFO-115	166	159	1.59
CFO-125	244	178	0.93
CFO-160	233	237	0.97
CFO-175	255	263	0.84
CFO-250	419	286	0.72
CFO-300	333	291	0.67

With a view of understanding the topography and surface roughness of the films, AFM measurements were carried out and are depicted in Fig. 3(g–l). The surface roughness values for the thin film samples are listed in Table 2. From the table it is evident that the surface roughness

Table 3
The different vibrational modes, cation distribution (at A- and B-sites), force constants (measured in dyne/cm), and magnetic moment (μ) of CFO films obtained from Raman spectra.

	CFO-115	CFO-125	CFO-160	CFO-175	CFO-250	CFO-300
$A_{1g}(1)$	694	691	695	693	691	692
$A_{1g}(2)$	678	662	679	677	675	670
$A_{1g}(3)$	619	616	622	617	614	617
$T_{2g}(1)$	183	179	171	176	170	170
$T_{2g}(2)$	457	456	457	454	454	457
$T_{2g}(2)$	477	475	476	473	473	477
$T_{2g}(3)$	567	570	573	569	572	575
E_g	305	306	306	305	304	305
$\frac{I(T_{2g}(2))}{I(A_{1g}(1))}$	0.489	0.619	0.522	0.535	0.676	0.471
A-site	$(Co_{0.281}Fe_{0.719})_T$	$(Co_{0.244}Fe_{0.756})_T$	$(Co_{0.295}Fe_{0.705})_T$	$(Co_{0.329}Fe_{0.671})_T$	$(Co_{0.258}Fe_{0.742})_T$	$(Co_{0.229}Fe_{0.770})_T$
B-site	$(Co_{0.719}Fe_{1.281})_O$	$(Co_{0.756}Fe_{1.244})_O$	$(Co_{0.705}Fe_{1.295})_O$	$(Co_{0.671}Fe_{1.326})_O$	$(Co_{0.742}Fe_{1.258})_O$	$(Co_{0.770}Fe_{1.229})_O$
$K_T \times 10^5$	2.08	2.06	2.09	2.08	2.06	2.06
$K_O \times 10^5$	1.13	1.13	1.13	1.12	1.12	1.13
μ (μ_B/f.u.)	4.12	3.98	4.18	4.32	4.03	3.92

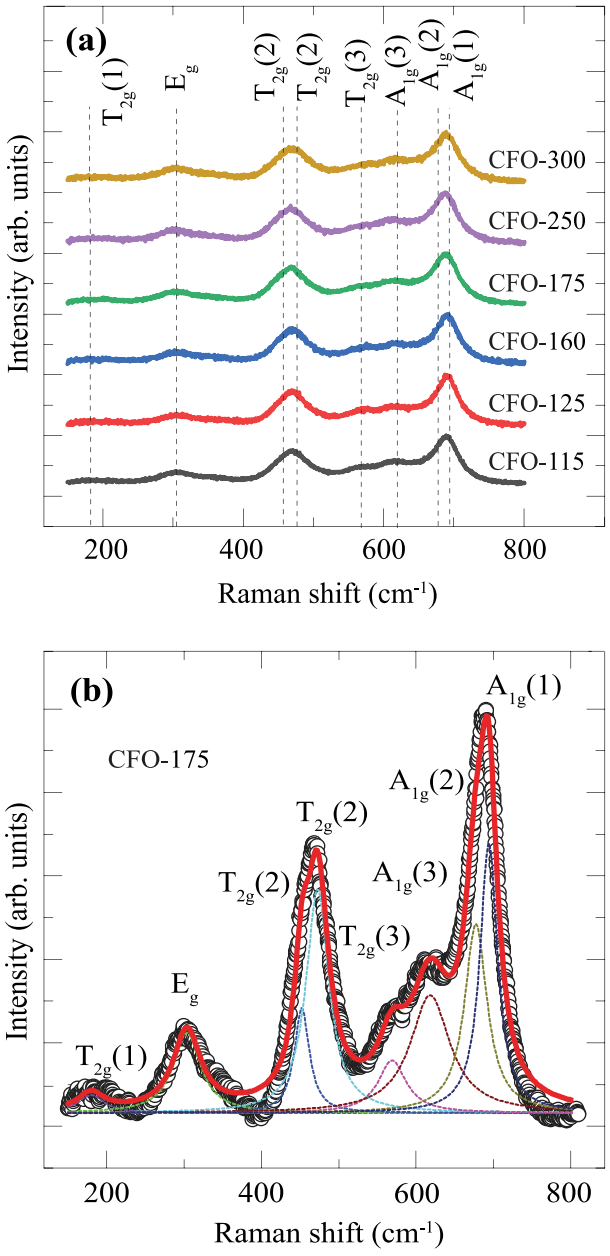

Fig. 4. (a) Raman spectra for CFO thin film samples and (b) de-convoluted Raman spectrum of CFO-175 sample.

decreases with increase in film thickness which is a consequence of the minimization of compressive strain. As the stray field nearby the dislocations may give rise to misfit dislocations in the thicker films, there will be a change in the surface morphology. The islands on film surfaces seen in AFM images occur when nucleation of dislocations happens, leading to roughness in the system. Thus the islands in AFM images is attributed to the dislocations, indicating the lattice relaxation occurring in the films [24].

3.3. Raman spectroscopy

Raman spectroscopy is a distinctive technique used to understand the various chemical species and their vibrational modes, thereby giving information about the crystal structure and physical properties exhibited by them. In the case of ferrites, it also can contribute to understanding the cation distribution in the materials. In this regard, Raman spectroscopy of all the thin films was carried out at RT in a frequency range 150–800 cm^{-1}, and the related spectra are shown in Fig. 4(a). According to the group theory analysis, the spinel cubic cobalt ferrite has 16 optical phonon modes, out of which 5 are Raman active viz., E_g, $3T_{2g}$ and A_{1g} [25,26]. The presence of these modes in the spectra with no peaks pertaining to any detectable secondary or impurity phases confirms the establishment of the cubic spinel phase of cobalt ferrite. It is in well agreement with the XRD analysis [27].

The vibrations of Fe and Co at the O_h and T_h sites give rise to peaks in the Raman spectra. To throw more light on the sub-lattice vibrations and the cation distribution for varying film thicknesses, the Lorentz profile fitting function was employed to de-convolute the Raman spectra and are presented in Fig. 4(b). The de-convoluted peak positions are listed in Table 3. The peak at 694 cm^{-1} represents the $A_{1g}(1)$ mode which is found to have 2 satellite peaks $A_{1g}(2)$ and $A_{1g}(3)$ around 680 cm^{-1} and 620 cm^{-1} respectively. These modes arise due to the symmetric stretching of O - Fe^{2+}, O - Fe^{3+} and O - Co^{2+} ions in the T_h site [28]. The peak identified around 170 cm^{-1} represents the $T_{2g}(1)$ mode corresponding to the translational motion of the metal cation which is in conjugation with the oxygen ions at the T_h site. The peak at 477 cm^{-1} is attributed to the $T_{2g}(2)$ vibrational mode, which results from the antisymmetric stretching of the O - Fe bond. However, the shoulder peak around 460 cm^{-1} is accounted to the antisymmetric stretching of the O - Co bond in the O_h sites. The $T_{2g}(3)$ mode observed around 570 cm^{-1} indicates the asymmetric bending of the O_h O - Fe bond. Also, the symmetric bending of O ions concerning the metal cations occurring at the O_h sites gives rise to the E_g vibrational mode as observed in the spectra [29–31]. The vibrational peaks in the spectra above 600 cm^{-1} are due to the T_h sublattice, and those below 600 cm^{-1} are due to the O_h sub-lattice vibrations [27–31]. As the intensity of the Raman peak is determined by the amount of cations present in the sub-lattice, the appearance of shoulder peaks indicate the existence of more

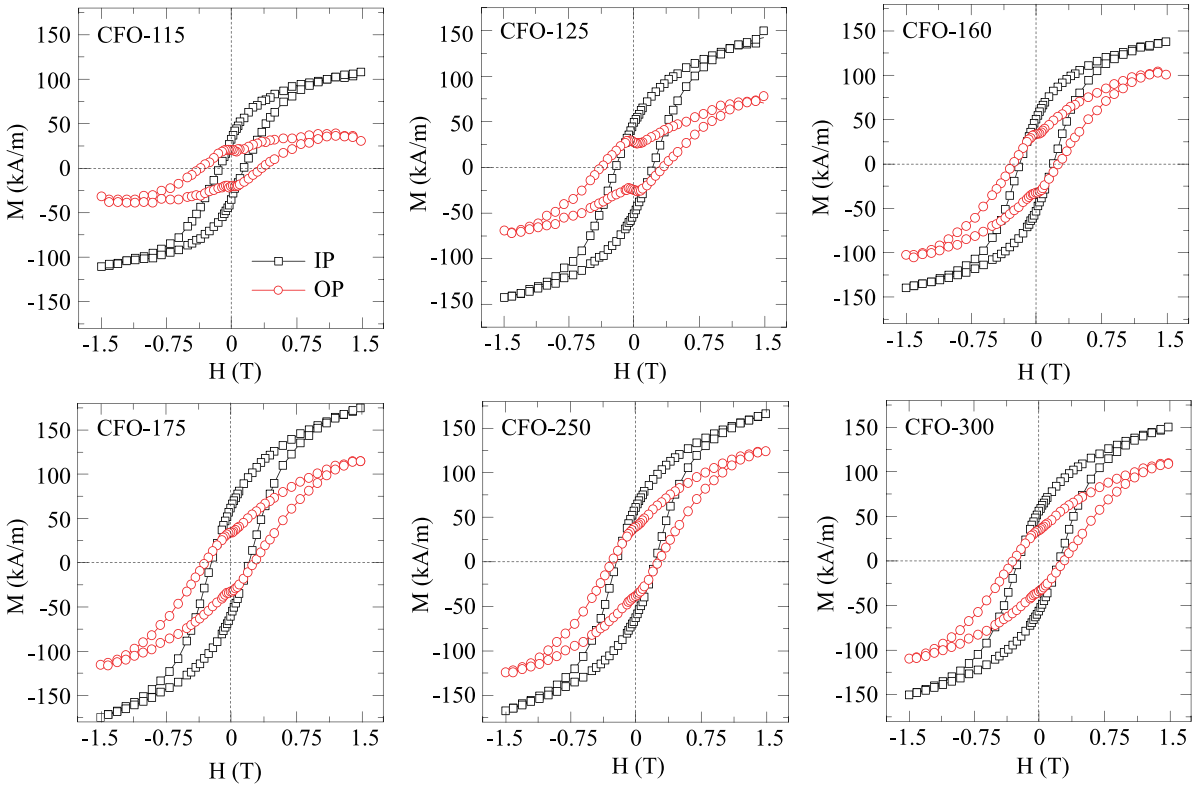

Fig. 5. The in-plane (IP) and out-of-plane (OP) $M-H$ curves of CFO thin film samples.

than one cation. Therefore the intensities and positions of $T_{2g}(2)$ and $A_{1g}(1)$, representing the O_h and T_h sites, respectively, were thoroughly analyzed. The ratio of the intensities of the above mentioned peaks are given in Table 3. The ratios were found to be nearly same for all the samples as they have the same chemical composition. The cation distribution of AB_2O_4 crystal structure at A and B sites was calculated from the peak intensities of the de-convoluted peaks and are given in Table 3. The estimated cation arrangement confirms the inverse spinel structure of the cobalt ferrite film samples. As the film thickness increases, there is an overall shift in the vibrational peaks towards the lower frequency side. This shift can be estimated from the peak force constant of the vibrating cation. As the frequency of vibration is found to be proportional to the force constant, the force constants of the T_h and O_h cations, K_T and K_O, respectively, were calculated from the equations [28,32],

$$K_T = 7.62 \times M_T \times \nu_T^2 \times 10^{-3} \tag{4}$$

$$K_O = 10.62 \times M_O \times \nu_O^2 \times 10^{-3} \tag{5}$$

where, M_T and M_O are the molecular weights of the ions present in the T_h and O_h sites, respectively, and ν_T and ν_O are the frequencies of the $A_{1g}(1)$ and E_g modes, respectively. The determined K_T and K_O values from the above equations are given in Table 3.

The K_T and K_O are found to have a random increase and decrease with the increase in thickness of the film. The force constant inversely varies with the bond length and affects the lattice parameter for ferrites. From the cation distribution, the magnetic moment of the films was calculated by,

$$\mu = m_B - m_A \tag{6}$$

where m_A and m_B are the magnetic moments of atoms at A and B sites, respectively, as per Neel's sub-lattice model. The enhancement in the magnetic moment from the expected value of bulk cobalt ferrite (3.31 μ_B) may be ascribed to the variation in the cation arrangement between the T_h and O_h sites [21].

3.4. Magnetization

With a view to understanding the magnetic behavior of the cobalt ferrite films, both IP and OP magnetic measurements ($M-H$) of all the samples were carried out at RT. The diamagnetic contribution was subtracted from the magnetization of the deposited films and the corresponding $M-H$ curves are presented in Fig. 5. The presence of a kink in the $M-H$ loop measured in OP near the zero-field region is worth mentioning. This can be related to the strain, which initiates an IP magnetic anisotropy due to the competing magnetocrystalline and shape anisotropies. The negative magnetostrictive behavior of the film may also be responsible for this observation [33]. This behavior is significant in thinner films compared to thicker ones, as the crystalline nature is more pronounced for thicker films. In addition, in the present case, the kink observed in $M-H$ loops at low fields indicates the presence of a minute secondary soft magnetic phase, likely to be magnetite, with a smaller H_C, which is a typical secondary phase often found in cobalt ferrite films. Due to the isostructural nature of magnetite with cobalt ferrite, XRD could not identify it as a secondary phase. The confirmation of the second phase requires a highly sophisticated characterization tool, which is beyond the scope of the present paper. It is well evident from the obtained graphs that the $M-H$ loops for both IP and OP show a change in H_C values and the technical saturation magnetization (M_{ST}) at 1.5 T as film thickness increases. Although the magnetic parameters are obtained from the minor $M-H$ loops, as the applied field is insufficient to saturate the magnetization of films, the variation of these parameters with film thickness is assumed to be unaffected in the present investigation. The variation in H_C and M_{ST} with respect to the thickness of film is depicted in Fig. 6(a, b). The variation of the H_C with film thickness for IP and OP are showing opposite variation up to film thickness of 175 nm. The large values of H_C for OP $M-H$ loops are attributed to the significant OP magnetization expected for thinner films in general. However, the variation of H_C for $M-H$ loops measured in IP is by the variation of H_C with particle size for nano/bulk cobalt ferrite materials [34].

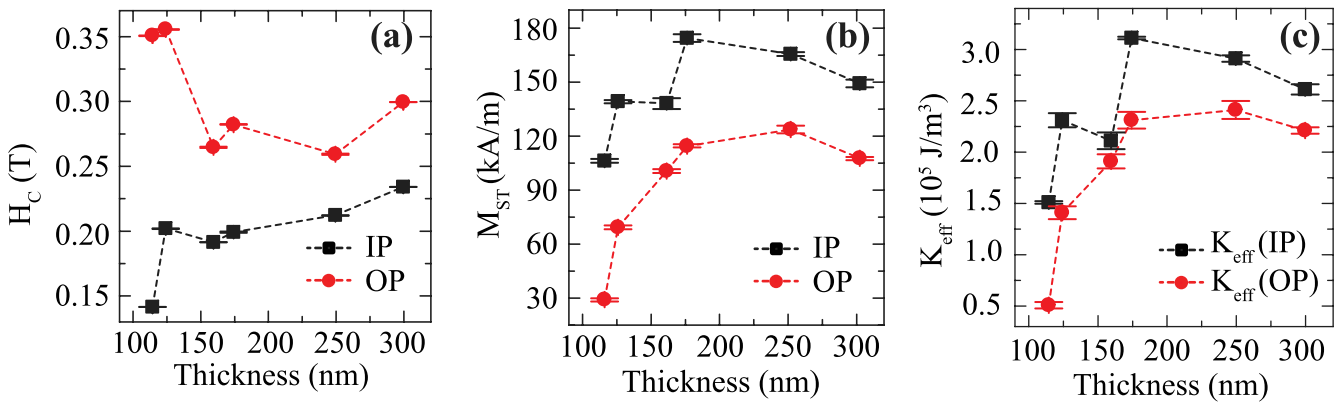

Fig. 6. The variation of (a) H_C, (b) M_{ST} and (c) K_{eff} with thickness of CFO thin film samples. The error bars represent the estimated standard deviation from the measurement of the corresponding parameter.

This observation follows the Stoner–Wohlfarth (SW) model of oriented uniaxial anisotropy. As per the SW model, the easy and hard axis of magnetization is IP and OP respectively [35]. The higher values of OP H_C also support this argument. Since the M_{ST} values of IP is greater than the OP, the cobalt ferrite films are having strong IP magnetic anisotropy [36]. The IP magnetization values are found to be comparable with the previous studies, and also, the IP and OP magnetizations are observed to be smaller than that of cobalt ferrite bulk (425 kA/m) [18].

Fig. 6(b) shows the variation of M_{ST} values for both IP and OP magnetization with film thickness. It is interesting to note from the Table 3 that the magnetic moment values calculated from Raman data are mimicking the M_{ST} values and its variation with film thickness. Since the magnetic moment obtained from Raman data is sensitive to the cation distribution, then the modulation in magnetization is a consequence of changes in the cation distribution. Therefore, this particular observation clearly ensures the establishment of structure–property correlations in cobalt ferrite thin films. However, the existence of a secondary soft magnetic phase and the degree of crystallization cannot be ignored in this case [33,36–39]. The IP and OP $M-H$ loops show a hysteric behavior due to the cubic anisotropy originating from the cubic symmetry associated with the bulk cobalt ferrite for an undistorted film lattice. Along with this, the shape anisotropy induces magnetization to be IP aligned, as evident from the $M-H$ loops [40].

As there is no saturation happening for the cobalt ferrite films in the range of applied field, the law of approach to saturation (LAS) was employed to estimate the saturation magnetization (M_S) and effective anisotropy constant (K_{eff}), which give a better understanding of the magnetic nature of the films. The equation corresponding to LAS is given as,

$$M = M_S\left(1 - \frac{b}{H^2}\right) \tag{7}$$

where, $\frac{b}{H^2}$ is the contribution from anisotropy. The above-mentioned equation was fitted to the experimentally obtained virgin curves for both IP and OP hysteresis loops. The parameter b obtained from the fitting can also be given by the equation,

$$b = 0.0762\left(\frac{K_{eff}^2}{\mu_0^2 M_S^2}\right) \tag{8}$$

where, K_{eff} and μ_0 are effective anisotropy constant and free space permeability, respectively. The K_{eff} values were calculated from the above equation, and the variation of K_{eff} with thickness for both IP and OP magnetization is shown in Fig. 6(c). It is clear from the figure that IP and OP magnetic anisotropy follow the same trend as H_C. In addition, there is a gradual rise in the OP M_{ST} and K_{eff} values with an increase in film thickness, as predicted from the increased OP magnetic contrast from the MFM analysis. Also, it is to be noted that the obtained anisotropy constant (IP and OP) for the films are much larger than the bulk cobalt ferrite values [34]. This significant difference in the values can be ascribed to the stress in the deposited thin films, originating from the mismatch between the film and substrate [41].

4. Conclusion

The oriented cobalt ferrite(111) thin films, with varying thickness, were deposited by using PLD technique. The XRD analysis confirms the formation of inverse spinel structure of cobalt ferrite and the growth of the films oriented along its [111] crystallographic direction. Due to the interface effects, the strain resulted in an increase in lattice parameters, confirming the lattice relaxation, and the thicker films tend to show the bulk behavior. The FESEM images confirm the existence of clusters known as the Stranski–Krastanov growth mechanism. The surface roughness of the films was found to decrease with the thickness due to lattice relaxations, which might also contribute to the above-mentioned growth mechanism. Hence, the AFM images again confirm the influence of strain on the film morphology. The Raman analysis identifies the vibrational modes in the samples. An agreement with the variation of magnetic moment (estimated from cation distribution) from the Raman data and technical saturation magnetization values from magnetization data as a function of film thickness ensures the structure–property correlations in cobalt ferrite thin films. The IP and OP $M-H$ data depict the reorientation of OP magnetization into IP with increasing thickness. The smaller values of IP H_C and the presence of a kink on the OP $M-H$ loops for thinner films establishes the strong IP magnetic anisotropy of the films and possibility of minute soft magnetic secondary phase in the films. The magnetic parameters associated with some of the samples widen the applicability of the cobalt ferrite thin films in suitable device applications at room temperature.

CRediT authorship contribution statement

Avisek Das: Sample preparation and characterization, Data collection and analysis, Manuscript (original draft) writing. **Annarose J Palliyan:** Data analysis, Manuscript writing. **Ajit Kumar Sahoo:** Sample characterization. **Jyoti Ranjan Mohanty:** Sample characterization. **Venkataiah Gorige:** Visualization, Conceptualization, Interpretation, Manuscript writing (review & editing), Funding acquisition.

Declaration of competing interest

The authors declare that they have no known competing financial interests or personal relationships that could have appeared to influence the work reported in this paper.

Data availability

Data will be made available on request.

Acknowledgments

The authors thank the Department of Science and Technology (DST) (Grant No. : DST/INT/JSPS/P-284/2019), India for awarding Indo-Japan joint research project, and Science and Engineering Research Board, DST (Grant No. : CRG/2020/001382), India for financial support. Also, the authors are thankful to the directorate of the Institute of Eminence, University of Hyderabad (Grant No. : UoH- IoE-RC3-21-007), India for the infrastructural and financial support.

References

[1] L. Caretta, E. Rosenberg, F. Büttner, T. Fakhrul, P. Gargiani, M. Valvidares, Z. Chen, P. Reddy, D.A. Muller, C.A. Ross, G.S.D. Beach, Interfacial Dzyaloshinskii-Moriya interaction arising from rare-earth orbital magnetism in insulating magnetic oxides, Nature Commun. 11 (2020) 1090, http://dx.doi.org/10.1038/s41467-020-14924-7.

[2] R. Ramesh, N.A. Spaldin, Multiferroics: progress and prospects in thin films, Nature Mater. 6 (2007) 21, http://dx.doi.org/10.1038/nmat1805.

[3] M. Cernea, B.S. Vasile, V.A. Surdu, R. Trusca, C. Bartha, F. Craciun, C. Galassi, Probing the dielectric, piezoelectric and magnetic behavior of $CoFe_2O_4$/BNT-$BT_{0.08}$ composite thin film fabricated by sol–gel and spin-coating methods, Sci. Rep. 8 (2018) 17883, http://dx.doi.org/10.1038/s41598-018-36232-3.

[4] S. Maat, M.J. Carey, Eric E. Fullerton, T.X. Le, P.M. Rice, B.A. Gurney, Cobalt–oxide underlayers for cobalt–ferrite pinned spin valves, Appl. Phys. Lett. 81 (2002) 520, http://dx.doi.org/10.1063/1.1494461.

[5] M.J. Carey, S. Maat, P. Rice, R.F.C. Farrow, R.F. Marks, A. Kellock, P. Nguyen, B.A. Gurney, Spin valves using insulating cobalt ferrite exchange-spring pinning layers, Appl. Phys. Lett. 81 (2002) 1044, http://dx.doi.org/10.1063/1.1494859.

[6] A. Lisfi, J.C. Lodder, E.G. Keim, C.M. Williams, Evidence of stress anisotropy and role of oxygen pressure in growth of pulsed-laser-deposited hexaferrite films, Appl. Phys. Lett. 82 (2003) 76, http://dx.doi.org/10.1063/1.1533854.

[7] M. Grigorova, H.J. Blythe, V. Blaskov, V. Rusanov, V. Petkov, V. Masheva, D. Nihtianova, L.M. Martinez, J.S. Muñoz, M. Mikhov, Magnetic properties and Mössbauer spectra of nanosized $CoFe_2O_4$ powders, J. Magn. Magn. Mater. 183 (1998) 163, http://dx.doi.org/10.1016/S0304-8853(97)01031-7.

[8] A.V. Ramos, T.S. Santos, G.X. Miao, M.J. Guittet, J.B. Moussy, J.S. Moodera, Influence of oxidation on the spin-filtering properties of $CoFe_2O_4$ and the resultant spin polarization, Phys. Rev. B 78 (2008) 180402, http://dx.doi.org/10.1103/PhysRevB.78.180402.

[9] G.D. Soria, K. Freindl, J.E. Prieto, A. Quesada, J. de la Figuera, N. Spiridis, J. Korecki, J.F. Marco, Growth and characterization of ultrathin cobalt ferrite films on Pt(111), Appl. Surf. Sci. 586 (2022) 152672, http://dx.doi.org/10.1016/j.apsusc.2022.152672.

[10] W. Weiss, W. Ranke, Surface chemistry and catalysis on well-defined epitaxial iron-oxide layers, Prog. Surf. Sci. 70 (2002) 1, http://dx.doi.org/10.1016/S0079-6816(01)00056-9.

[11] G.S. Parkinson, Iron oxide surfaces, Surf. Sci. Rep. 71 (2016) 272, http://dx.doi.org/10.1016/j.surfrep.2016.02.001.

[12] L.M. Garcia, A. Quesada, C. Munuera, J.F. Fernández, M.G. Hernández, M. Foerster, L. Aballe, J. de la Figuera, Atomically flat ultrathin cobalt ferrite islands, Adv. Mater. 27 (2015) 5955, http://dx.doi.org/10.1002/adma.201502799.

[13] J. Ding, Y.J. Chen, Y. Shi, S. Wang, High coercivity in SiO_2-doped $CoFe_2O_4$ powders and thin films, Appl. Phys. Lett. 77 (2000) 3621, http://dx.doi.org/10.1063/1.1328374.

[14] S.C. Sahoo, N. Venkataramani, S. Prasad, M. Bohra, R. Krishnan, Thickness dependent anomalous magnetic behavior in pulsed-laser deposited cobalt ferrite thin film, Appl. Phys. A 106 (2012) 931, http://dx.doi.org/10.1007/s00339-011-6709-1.

[15] R. Patel, T. Tainosho, Y. Hisamatsu, S. Sharmin, E. Kita, H. Yanagihara, Effect of lattice strain on cobalt ferrite $Co_{0.75}Fe_{2.25}O_4$ (111) thin films, Japan. J. Appl. Phys. 56 (2017) 053001, http://dx.doi.org/10.7567/JJAP.56.053001.

[16] Y.C. Wang, J. Ding, J.B. Yi, B.H. Liu, T. Yu, Z.X. Shen, High-coercivity Co-ferrite thin films on (100)-SiO_2 substrate, Appl. Phys. Lett. 84 (2004) 2596, http://dx.doi.org/10.1063/1.1695438.

[17] W. Huang, J. Zhu, H.Z. Zeng, X.H. Wei, Y. Zhang, Y.R. Lia, Strain induced magnetic anisotropy in highly epitaxial $CoFe_2O_4$ thin films, Appl. Phys. Lett. 89 (2006) 262506, http://dx.doi.org/10.1063/1.2424444.

[18] M. Khodaei, S.A.S. Ebrahimi, Y.J. Park, J.M. Ok, J.S. Kim, J. Son, S. Baik, Strong in-plane magnetic anisotropy in (111)-oriented $CoFe_2O_4$ thin film, J. Magn. Magn. Mater. 340 (2013) 16, http://dx.doi.org/10.1016/j.jmmm.2013.03.019.

[19] R.K. Mishra, G. Thomas, Surface energy of spinel, J. Appl. Phys. 48 (1977) 4576, http://dx.doi.org/10.1063/1.323486.

[20] S. Dolabella, A. Borzí, A. Dommann, A. Neels, Lattice strain and defects analysis in nanostructured semiconductor materials and devices by High-Resolution X-ray diffraction: theoretical and practical aspects, Small Methods 6 (2022) 2100932, http://dx.doi.org/10.1002/smtd.202100932.

[21] K.K. Bestha, J.J. Abraham, J.A. Chelvane, V. Gorige, Influence of cation distribution on magnetic response of polycrystalline $Co_{1-x}Ni_xFe_2O_4$ ($0 \le x \le 1$) ferrites, Phys. Scr. 95 (2020) 085802, http://dx.doi.org/10.1088/1402-4896/aba3d2.

[22] V.M. Kumar, A. Srinivas, A. Talapatra, S. Asthana, J. Mohanty, S.V. Kamat, Effect of deposition temperature on structural, microstructural and magnetic properties of $CoFe_2O_4$ thin films deposited by pulsed laser deposition, J. Mater. Sci.: Mater. Electron. 28 (2017) 446, http://dx.doi.org/10.1007/s10854-016-5541.

[23] Z. Chen, C.H. Shek, J.K.L. Lai, Insights into microstructural evolution and polycrystalline compounds formation from Pd–Ge thin films, Phys. B: Condens. Matter 358 (2005) 56, http://dx.doi.org/10.1016/j.physb.2004.12.026.

[24] R. Comes, M. Gu, M. Khokhlov, J. Lu, S.A. Wolf, Microstructural and domain effects in epitaxial $CoFe_2O_4$ films on MgO with perpendicular magnetic anisotropy, J. Magn. Magn. Mater. 324 (2012) 4, http://dx.doi.org/10.1016/j.jmmm.2011.08.033.

[25] P. Chand, S. Vaish, P. Kumar, Structural, optical and dielectric properties of transition metal (MFe_2O_4; M=Co, Ni and Zn) nanoferrites, Phys. B 524 (2017) 53, http://dx.doi.org/10.1016/j.physb.2017.08.060.

[26] G.P. Nethala, R. Tadi, G.R. Gajula, P.V.P. Madduri, A.V. Anupama, V. Veeraiah, Influence of Cr on structural, spectroscopic and magnetic properties of $CoFe_2O_4$ grown by the wet chemical method, Mater. Chem. Phys. 238 (2019) 121903, http://dx.doi.org/10.1016/j.matchemphys.2019.121903.

[27] S. Thota, S.C. Kashyap, S.K. Sharma, V.R. Reddy, Cation distribution in Ni-substituted $Mn_{0.5}Zn_{0.5}Fe_2O_4$ nanoparticles: A Raman, Mössbauer, X-ray diffraction and electron spectroscopy study, Mater. Sci. Eng. B 206 (2016) 69, http://dx.doi.org/10.1016/j.mseb.2016.01.002.

[28] B. Nandan, M.C. Bhatnagar, S.C. Kashyap, Cation distribution in nanocrystalline cobalt substituted nickel ferrites: X-ray diffraction and Raman spectroscopic investigations, J. Phys. Chem. Solids 125 (2019) 298, http://dx.doi.org/10.1016/j.jpcs.2019.01.017.

[29] A. Kumar, P. Sharma, D. Varshney, Structural, vibrational and dielectric study of Ni doped spinel Co ferrites: $Co_{1-x}Ni_xFe_2O_4$ (x=0.0, 0.5, 1.0), Ceram. Int. 40 (2014) 12855, http://dx.doi.org/10.1016/j.ceramint.2014.04.140.

[30] J. Jacob, M.A. Khadar, Investigation of mixed spinel structure of nanostructured nickel ferrite, J. Appl. Phys. 107 (2010) 114310, http://dx.doi.org/10.1063/1.3429202.

[31] P.N. Anantharamaiah, P.A. Joy, Effect of size and site preference of trivalent non-magnetic metal ions (Al^{3+}, Ga^{3+}, In^{3+}) substituted for Fe^{3+} on the magnetostrictive properties of sintered $CoFe_2O_4$, J. Phys. D: Appl. Phys. 50 (2017) 435005, http://dx.doi.org/10.1088/1361-6463/aa8af6.

[32] R.D. Waldron, Infrared spectra of ferrites, Phys. Rev. 99 (1955) 1727, http://dx.doi.org/10.1103/PhysRev.99.1727.

[33] D. Mukherjee, M. Hordagoda, R. Hyde, N. Bingham, H. Srikanth, S. Witanachchi, P. Mukherjee, Nanocolumnar interfaces and enhanced magnetic coercivity in preferentially oriented cobalt ferrite thin films grown using oblique-angle pulsed laser deposition, Appl. Mater. Interfaces 5 (2013) 7450, http://dx.doi.org/10.1021/am401771z.

[34] A. Das, K.K. Bestha, B. Prakash, V. Gorige, Correlation between size, shape and magnetic anisotropy of $CoFe_2O_4$ ferrite nanoparticles, Nanotechnology 31 (2020) 335716, http://dx.doi.org/10.1088/1361-6528/ab8fe8.

[35] E.C. Stoner, E.P. Wohlfarth, A mechanism of magnetic hysteresis in heterogeneous alloys, Phil. Trans. R. Soc. A 240 (1948) 826, http://dx.doi.org/10.1098/rsta.1948.0007.

[36] M. Khodaei, S.A.S. Ebrahimi, Y.J. Park, S.H. Choi, Thickness dependent magnetic properties of (111)-oriented $Co_{0.8}Fe_{2.2}O_4$ thin film grown by pulsed laser deposition, Thin Solid Films 571 (2014) 62, http://dx.doi.org/10.1016/j.tsf.2014.09.062.

[37] T. Niizeki, Y. Utsumi, R. Aoyama, H. Yanagihara, J. Inoue, Y. Yamasaki, H. Nakao, K. Koike, E. Kita, Extraordinarily large perpendicular magnetic anisotropy in epitaxially strained cobalt-ferrite $Co_xFe_{3-x}O_4$(001) (x=0.75, 1.0) thin films, Appl. Phys. Lett. 103 (2013) 162407, http://dx.doi.org/10.1063/{1}.4824761.

[38] F. Rigato, J. Geshev, V. Skumryev, J. Fontcuberta, The magnetization of epitaxial nanometric $CoFe_2O_4$(001) layers, J. Appl. Phys. 106 (2009) 113924, http://dx.doi.org/10.1063/1.3267873.

[39] R. Lin, J.H. Liao, L.J. Hung, T.B. Wu, Effect of the $CoFe_2O_4$ thin film thickness on multiferroic property of (00l)-oriented $Pb(Zr_{0.5}Ti_{0.5})O_3$/$CoFe_2O_4$/$Pb(Zr_{0.5}Ti_{0.5})O_3$ trilayer structure, J. Appl. Phys. 103 (2008) 07320, http://dx.doi.org/10.1063/1.2839313.

[40] A. Lisfi, C.M. Williams, L.T. Nguyen, J.C. Lodder, A. Coleman, H. Corcoran, A. Johnson, P. Chang, A. Kumar, W. Morgan, Reorientation of magnetic anisotropy in epitaxial cobalt ferrite thin films, Phys. Rev. B. 76 (2007) 054405, http://dx.doi.org/10.1103/PhysRevB.76.054405.

[41] T. Dhakal, D. Mukherjee, R. Hyde, P. Mukherjee, M.H. Phan, H. Srikanth, S. Witanachchi, Magnetic anisotropy and field switching in cobalt ferrite thin films deposited by pulsed laser ablation, J. Appl. Phys. 107 (2010) 053914, http://dx.doi.org/10.1063/1.3327424.